Journal of Catalysis **185,** 33–42 (1999)
Article ID jcat.1999.2480, available online at http://www.idealibrary.com on IDEAL®

Enhanced *para*-Selectivity by Selective Coking during Toluene Disproportionation over H–ZSM-5 Zeolite

Liang-Yuan Fang,* Shang-Bin Liu,† and Ikai Wang*,[1]

*Department of Chemical Engineering, National Tsinghua University, Hsinchu, Taiwan 300, Republic of China; and †Institute of Atomic and Molecular Sciences, Academia Sinica, P.O. Box 23-166, Taipei, Taiwan 106, Republic of China

Received May 28, 1998; revised March 12, 1999; accepted March 15, 1999

A coke selectivation process, i.e., modification of selectivity, was divided into five separate stages. Each stage was under either N_2 or H_2 as the carrier gas and at different reaction temperatures for various time-on-stream. The spent sample obtained during each stage was characterized by a combination of different techniques, namely thermogravimetric analysis, temperature programmed desorption of ammonia, xenon adsorption, X-ray photoelectron, and ^{129}Xe NMR spectroscopy. In the presence of N_2 carrier gas, the carbonaceous deposits formed within the intracrystalline channels were mostly light volatile soft coke, which was effectively removed by a succeeding treatment with H_2 gas. On the other hand, bulkier, more condensed hard coke was formed on the external surface of the zeolite crystallites and is more difficult to be removed by simple hydrogen treatment. After the five-stage selectivation process, most of the coke is found to be on the external surface of the catalyst. As a result, the isomerization of the primary product, *para*-xylene, was retarded. The *para*-selectivity was found to increase from ca. 24 to 49% at a slight expense of conversion. A detailed reaction mechanism for the *para*-selectivity enhancement during the five-stage coke selectivation process is proposed.

Key Words: **H–ZSM-5; coke; *para*-selectivity; regeneration; toluene disproportionation.**

INTRODUCTION

Coking is the primary reason for zeolite deactivation during hydrocarbon acid-catalyzed reactions. Extensive research has been done on coking and deactivation of zeolite catalysts (1–18) and the subject has been comprehensively reviewed (19–22). Earlier studies focused mostly on the effect of the type and morphology of the catalyst used (1, 7–11), the nature, location, and formation mechanism of coke (6, 7, 11–15), and the reaction parameters (8–10, 13). Relatively few studies were made on related topics such as catalyst regeneration (12, 18), coke induced selectivation (13, 24) or carrier gas effect (25–29). For the latter, while the correlation between carrier gas concentration and initial conversion and/or deactivation rate of the catalyst has been reported, the differences among different carrier gases were discussed in few details. Moreover, the relevant effects of carrier gas were sometimes neglected. For example, inert carrier gases such as He, N_2, or Ar are generally considered only as a diluent which serves to ease the transport of reactants and products through the catalyst.

Chen *et al.* (25) proposed a solvation model of a transition complex for cumene disproportionation over zeolite beta in the presence of various carrier gases, viz. N_2, H_2, He, and CO_2. The authors concluded that a combination of physical and van der Waals interactions of carrier gas molecules with the reaction intermediates and product molecules must be used to describe the observed catalytic activity and stability of the catalyst during cumene disproportionation over zeolite beta through a bimolecular (S_{N2}) reaction mechanism. Bauer *et al.* (30) studied the reactivation of fouled H–ZSM-5 catalyst, obtained from the conventional methanol to gasoline (MTG) reaction, by treating the catalyst with H_2 and light alkanes. They pointed out that the presence of these carrier gases provokes catalyst regeneration while maintaining the desired selectivity.

Improving the *para*-xylene yield from toluene disproportionation is an important industrial issue. Mobil researchers have developed a special coking pretreatment process on ZSM-5 catalyst that largely enhances the *para*-selectivity at a slight expense of conversion (31–39). The so-called Mobil Selective Toluene Disproportionation Process (MSTDP) which was first commercialized in 1988 (35) invoked reaction temperature variation and selective reactivation by using H_2 as a regenerating gas. However, the details of the coking pretreatment procedure are lacking and the mechanism of coke selectivation (i.e., modification of selectivity) remains uncertain.

We have designed a multistage procedure of catalyst coking pretreatment to investigate the effect of coke deposition on the activity and selectivity of H–ZSM-5 zeolite during toluene disproportionation. The variation in conversion and selectivity in each stage was monitored. Various analytic methods such as temperature-programmed desorption of ammonia (NH_3-TPD), xenon adsorption isotherm

[1] To whom correspondence should be addressed.

0021-9517/99 $30.00

TABLE 1

Reaction Conditions and Characteristics of the Coked Samples Obtained from the Five-Stage Coke Selectivation Process and Control Reactions[a]

	Coke selectivation process[b]					Control reactions			
Stage of reaction	I	II	III	IV	V	I'	II'	III'	IV'
Sample notation[c]	S1	S2	S3	S4	S5	T1	T2	T3	T4
Temperature (K)	753	753	813	813	753	753	753	813	813
Carrier gas	N_2	H_2	N_2	H_2	H_2	N_2	H_2	N_2	H_2
Time-on-stream (h)	24	4	69	9	19	480	170	44	120
Residual acidity (%)[d]	54.8	66.3	~0	63.2	51.0	52.7	97.4	~0	68.2
Coke content (wt%)[e]	7.2	5.3	26.2	18.3	18.8	53.0	3.1	24.5	5.7
C/Si ratio[f]	1.6	1.0	9.6	7.6	8.2	7.7	0.9	6.0	1.2
$(\sigma_{xe})_{coked}$[g]	5.76	5.14	40.71	5.44	5.45	10.87	5.43	32.59	5.45
V/V_o (%)[h]	88.5	99.2	12.5	93.8	93.6	46.9	93.9	15.6	93.6

[a] All reactions were carried out at pressure (2.76 MPa); carrier gas to feed ratio 4 mol/mol; WHSV 6.5 h^{-1}.

[b] Samples were labeled based on the stage at which feeding was stopped.

[c] The dehydrated (573K; over 20 h) fresh zeolite sample is denoted by S0.

[d] Obtained from the strong acid sites of the NH_3-TPD profiles (Fig. 6). The values were calculated by the ratio of the peak areas obtained from the coked and fresh samples. The number of the strong acid sites for the fresh catalyst, taken as 100%, is ca. 320 μmole/g.

[e] Obtained from TGA results.

[f] Obtained from XPS results.

[g] Obtained from the slope of the $\delta(\rho)$ vs ρ plot in Fig. 5; in unit of 10^{-20} ppm g cat. $atom^{-1}$.

[h] Calculated by Eq. [3], taking $(\sigma_{xe})_{fresh} = 5.10 \times 10^{-20}$ ppm g cat. $atom^{-1}$ observed for the fresh ZSM-5 zeolite (sample S0).

measurement, thermogravimetric analysis (TGA), ^{129}Xe NMR, and X-ray photoelectron spectroscopy (XPS) were employed to unveil the phenomena related to coke selectivation.

EXPERIMENTAL

The composition and the framework structure of the H–ZSM-5 zeolite (Si/Al = 34; obtained from Strem Chemical, Inc.) were confirmed by ICP-AES and powder X-ray diffraction, respectively. The particle size of the powdered sample was about 0.3–0.5 μm as observed by electron microscopy. Toluene (L.C. grade) was obtained from ALPS Chemical Company and was used without further purification.

All reactions were conducted in a continuous flow, fixed-bed reactor (stainless steel; 15 mm i.d.). The pressed and pelletized zeolite sample (12–20 mesh; ca. 1.8 g) was mixed with quartz (ca. 10–12 mesh) and packed into the reactor. Prior to the reaction, the sample was calcined in air at 823 K for 8 h. The reactor was then cooled in a flowing N_2 atmosphere down to the desired reaction temperature.

To obtain identical contact times for each run, all reactions were carried out at a pressure of 2.76 MPa, a carrier gas to feed (CGF) ratio of 4 mol/mol and a space velocity (WHSV) of 6.5 h^{-1}. In order to investigate the effect of coke (e.g., nature, amount, and location of coke) on the catalytic performance (conversion and *para*-selectivity), the entire selectivation process was divided into five stages. Each stage has a set temperature and carrier gas. The conditions and characteristics of each stage are presented in Table 1.

Stage I had a low reaction temperature (753 K) and used N_2 as the carrier gas. In Stage II, while the reaction temperature was unchanged, H_2 was used as the carrier gas. Since mild coking is expected to occur during Stage I, the presence of H_2 during Stage II for 4 h was considered adequate to reactivate the aged catalyst. During Stage III, the carrier gas was switched from H_2 to N_2 while the reaction temperature was raised from 753 to 813 K and the TOS extended to 69 h. The carrier gas was switched back to H_2 during Stage IV while maintaining the reaction temperature from the previous stage (III). Since a more severe coking is expected to occur during Stage III, the TOS was prolonged to 9 h to provoke catalyst regeneration. In the final stage (V), the reaction temperature was lowered to 753 K while keeping H_2 as the carrier gas for a TOS of 19 h. Such reaction conditions render possible a convenient comparison of the data, such as conversion and *para*-selectivity, with those obtained during Stages I and II.

A sample was obtained at the conclusion of each stage. Hence a total of five samples was collected. Before unloading the sample, feeding was stopped at the end of the respective stage and then the system was purged under the same reaction conditions (i.e., same temperature and carrier gas) for more than 8 h to remove the unreacted reagents and products. Samples were labeled based on the stage at which feeding was stopped (Table 1).

Thermogravimetric analysis (TGA) was conducted on a Seiko SSC500-TG thermogravimeter under the following

TABLE 2

Catalytic Performance and Effluent Distribution during the Five-Stage Process for Toluene Disproportionation over H–ZSM-5 Zeolite (WHSV = 6.5 h^{-1}, Carrier Gas/Toluene Feed = 4 mol/mol)

Stage	I		II		III		IV		V	
TOS (h)	1	24	25	28	29	97	98	106	107	125
Conversion (wt%)	44.8	38.2	43.0	43.9	52.1	5.3	29.2	45.0	34.7	33.0
Effluent distribution (wt%)										
Benzene	19.5	15.6	17.4	17.2	24.6	2.2	14.0	22.7	16.3	14.8
Toluene	55.2	61.8	57.0	56.1	47.9	94.7	70.8	55.0	65.3	67.0
Ethylbenzene	0.2	0.1	0.4	0.4	0.5	0.0	0.4	1.0	0.2	0.2
Xylenes	24.7	21.7	23.5	24.7	24.8	3.1	14.3	20.4	17.1	17.1
Others	0.4	0.8	1.7	1.6	2.2	0.0	0.5	0.9	1.1	0.9
Xylene isomers (%)										
p-xylene	24.1	24.1	24.0	23.7	23.5	47.5	57.0	38.0	48.5	48.7
m-xylene	50.7	50.9	49.7	50.1	50.5	38.1	31.7	46.5	39.6	39.8
o-xylene	25.2	25.0	25.3	26.2	26.0	14.4	11.3	15.5	11.9	11.5

conditions: sample weight, 50 mg; flowing gas, air; reference sample, platinum; heating rate, 10 K min^{-1}; and final temperature, 1073 K. Temperature-programmed desorption (TPD) of NH_3 was carried out on a thermosorption system using a thermal conductivity detector. Prior to the adsorption of NH_3, the system was preheated at 573 K under dried He gas for 1 h and then cooled to 373 K. After the complete removal of physisorbed NH_3 by purging, the TPD profile of the sample was recorded with a heating rate 10 K min^{-1} to a temperature as high as 823 K.

For the Xe adsorption and ^{129}Xe NMR experiments, the sample (ca. 0.8 g) was placed in a standard 10 mm NMR tube connected to a coaxial Teflon stopcock. The sample tube design not only provided a convenient connection to the vacuum manifold but also facilitated sample dehydration and gas adsorption. For dehydration, the sample temperature was slowly raised (1 K min^{-1}) to 573 K and maintained at that temperature for at least 20 h under vacuum ($<1.33 \times 10^{-3}$ Pa). Xenon adsorption isotherms were recorded at room temperature (297 K). The equilibrium pressures of xenon were measured using an absolute pressure transducer (MKS Baratron). ^{129}Xe NMR experiments were performed on a Bruker MSL-300P NMR spectrometer operating at 83.012 MHz. Typically, 50–20,000 free induction decay signals were accumulated (depending on the xenon coverage, θ) with a recycle delay of 0.3 s. The reference for the ^{129}Xe NMR chemical shift was that of diluted Xe gas. ^{27}Al magic-angle-spinning (MAS) NMR experiments were performed for the fresh and the spent catalysts. The ^{27}Al MAS NMR spectra were recorded at 78.21 MHz using a single-pulse scheme with a recycle delay of 0.3 s and a sample spinning frequency ca. 5 kHz. All samples showed nearly no trace of extraframework Al indicating that the crystalline structure of the zeolite remains practically unchanged throughout the reaction process. In order to further clarify the existence of "NMR invisible" Al species, samples treated with acetylacetone (for 5 days) were also examined (40–42). However, no trace of "invisible Al" was found in either the fresh or the spent catalysts.

XPS measurements were conducted on a Perkin Elmer PHI1600 XPS system operating at a working pressure of 1.33×10^{-7} Pa. All spectra were recorded using Mg $K\alpha$ excitation with a scanning width spanning between 0 and 1.25 keV. The peak areas were determined by individual scans over a 12.5 eV range from 73 eV (Al), 102 eV (Si), and 282 eV (C), respectively. The C/Si ratio was then determined from the integrated peak areas.

RESULTS AND DISCUSSION

The results obtained from toluene disproportionation over H–ZSM-5 zeolite are shown in Table 2. The variations in toluene conversion and *para*-xylene selectivity with TOS during the whole five-stage selectivation process are depicted in Fig. 1. The selectivity of *para*-xylene can be defined by the following equation:

$$\textit{para}\text{-selectivity} = (p\text{-xylene}/(\text{Sum of } p\text{-, } m\text{-, and } o\text{-xylene})) \times 100\%. \quad [1]$$

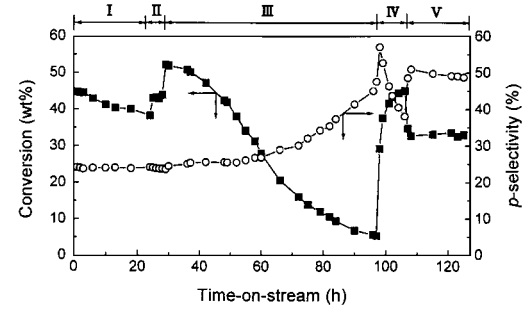

FIG. 1. Variations of toluene conversion and *para*-xylene selectivity with time-on-stream during the five-stage coke selectivation process of toluene disproportionation over H–ZSM-5 zeolite.

It is noted that the observed conversion and *para*-selectivity both show a distinct behavior during each stage of the reaction. In State I, the conversion is found to decrease monotonously with TOS whereas the *para*-selectivity remained constant. When the carrier gas was switched from N_2 to H_2 in Stage II, the activity rapidly restored to its initial value while the *para*-selectivity remained practically unchanged. At the beginning of Stage III, the gradual decrease in conversion may be ascribed as due to coke build-up. As a result, the *para*-selectivity remained at around 24% for TOS $<$ 40 h (Fig. 1). For TOS $>$ 40 h, a rapid decrease in conversion and gradual increase in *para*-selectivity was observed. At the end of Stage III, the conversion fell to its lowest value of 5.3 wt%, the observed value for *para*-selectivity on the other hand increased to ca. 47.5%.

Upon replacing the N_2 carrier gas by H_2 in Stage IV, the activity of the catalyst was restored rapidly and eventually reached a conversion value of ca. 45 wt% at the end of the stage. We note that such a high conversion is comparable to its initial conversion found in Stage I. On the other hand, the *para*-selectivity decreases from its optimal value (ca. 54%) to ca. 38% at the end of Stage IV. This *para*-selectivity, however, is still higher than that obtained at the beginning of Stage III (ca. 24%). The H_2 carrier gas, therefore, served as an effective medium to restore the activity of the H–ZSM-5 catalyst during toluene disproportionation. In Stage V, as the system remained under H_2 environment, the reaction temperature was lowered to 753 K. Both the conversion and the *para*-selectivity reached their plateau values. It can thus be concluded that, throughout the five-stage selectivation process, while the overall conversion decreased by ca. 11.8 wt% (from its initial value of 44.8 wt%), the overall *para*-selectivity was enhanced by ca. 24.6% (from 24.1 to 48.7%). This enhancement corresponds to a net increase in *para*-xylene yield of ca. 2.4 wt%. The five-stage coke selectivation process, therefore, resulted in a marked increase in *para*-selectivity. Such selectivity enhancement is not found when O_2-containing gas is used for regeneration. Nonetheless, the genuine role of the H_2 carrier gas as well as the detailed mechanism for selective regeneration need to be explored further.

To confirm the effects of carrier gas and reaction temperature on the *para*-selectivity enhancement, four control experiments, each with a fixed carrier gas and reaction temperature, were separately conducted for extended TOS. The purpose of performing these tests was to mimic each of the first four stages of the five-stage process. The carrier gas and the reaction temperature were both kept unchanged during each control experiment (denoted by I', II', III', and IV'). The sample numbers (denoted T1 to T4) and corresponding reaction conditions for these experiments are shown in Table 1. The catalytic results obtained from these tests are depicted in Fig. 2. The results show that, in the presence of N_2 (samples T1 and T3), the deactivation rate of toluene conversion increases with increasing reaction temperature. A closer examination of the results in Figs. 2a and 2c further reveals that, as the reaction temperature is increased

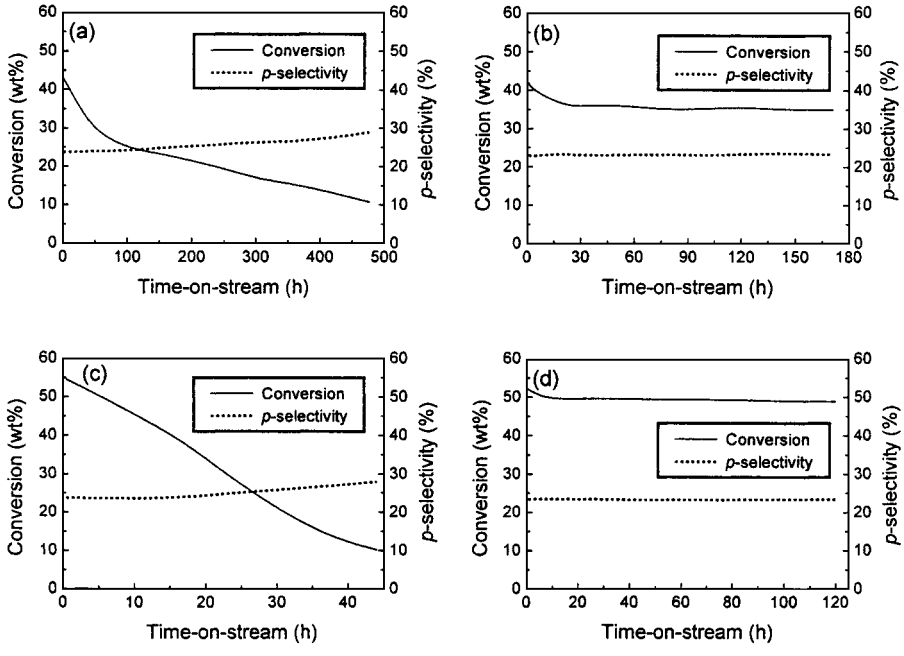

FIG. 2. Variations of conversion and *para*-selectivity with time-on-stream during toluene disproportionation control experiments over H–ZSM-5 zeolite. Each experiment was carried out at a specific temperature and carrier gas: (a) 753 K; N_2, (b) 753 K; H_2, (c) 813 K; N_2, and (d) 813 K; H_2, denoted by sample numbers T1 to T4, respectively (Table 1).

from 753 to 813 K, the initial (TOS < 40 h) deactivation rate is increased by more than three-fold. Moreover, for deactivation under a N_2 environment, no significant change in *para*-selectivity is found when the toluene conversion level is above 25 wt%. On the other hand, regardless of the reaction temperature, no apparent variations are found for both conversion and *para*-selectivity when under a H_2 environment (samples T2 and T4; cf. Figs. 2b and 2d) even for a TOS of up to 170 h.

Using TGA, the coke content for each sample can be deduced from the relative weight loss within the temperature range 673–1073 K of the thermogram, and the results are shown in Table 1. It is observed that the coke contents of samples T2 and T4 are a lot smaller than that of samples T1 and T3. Furthermore, the coke residues in samples S1 and S3 were reduced significantly by subsequent H_2 treatment (cf. samples S2 and S4). These results reveal that, compared to N_2, H_2 is more effective in retarding coke formation and/or removing the existing soft coke (*vide infra*) from the catalysts.

The xenon adsorption isotherms of the spent catalysts are shown in Fig. 3 together with that of the dehydrated fresh catalyst (sample denoted by S0). Assuming that the carbonaceous deposits themselves were not porous, the corresponding xenon loading for each sample can be determined by the amount of Xe adsorbed divided by the weight of the catalyst. The latter may be obtained by deducting the total coke content from the weight of the spent sample. The Langmuir-type isotherms in Fig. 3a indicate that both the adsorption strength and the capacity of the samples S2, S4, and S5 are similar to that of the fresh catalyst (S0). However, compared to S0, a slight decrease in the adsorption capacity was found for S1 and a drastic decrease was found for S3. The above results indicate that coke located in the intracrystalline channels of ZSM-5 zeolite can be effectively removed in the presence of H_2. A similar conclusion may be deduced from samples obtained from the control experiments (Fig. 3b). However, for these samples (S1–S4), while their sorption capacities follow the expected trend, a notable decrease is found for all samples compared to the fresh catalyst. This is mainly due to the prolonged TOS applied during the control experiments.

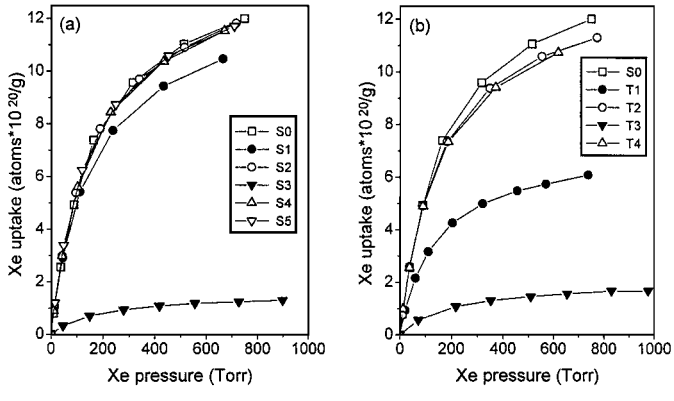

FIG. 3. The xenon adsorption isotherms at room temperature for fresh and coked samples obtained from (a) the five-stage process and (b) the control experiments. The detailed reaction conditions and the corresponding sample numbers are defined in Table 1.

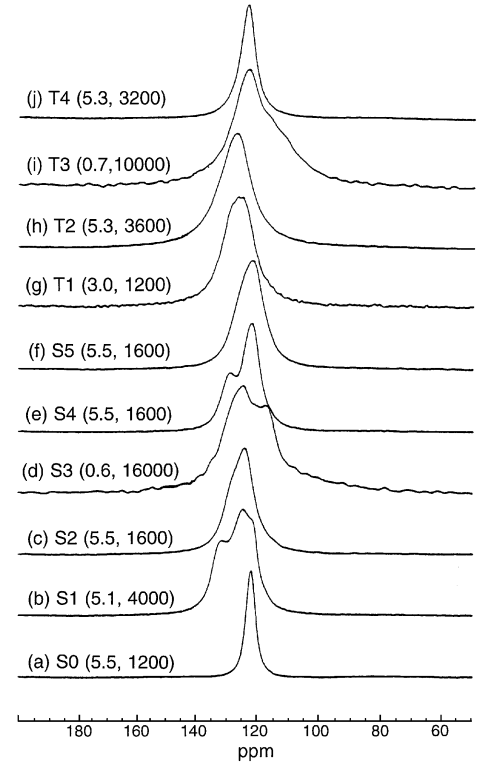

FIG. 4. Room temperature ^{129}Xe NMR spectra of xenon (equilibrium pressure 1.33×10^4 Pa) adsorbed on the fresh and coked samples. The detailed reaction conditions and the corresponding sample notations are given in Table 1. The values in parentheses following the sample number represent (θ, NS), where θ is the corresponding xenon coverage (in unit of 10^{20} atoms/g · cat.; obtained from Fig. 3) and NS is the number of signal accumulations, respectively.

Figure 4 displays the ^{129}Xe NMR spectra of xenon (equilibrium pressure 1.33×10^4 Pa) adsorbed on various samples. The spectrum of the fresh (dehydrated) sample is also shown for comparison in Fig. 4a. All spectra obtained from the spent samples show broader lines and higher chemical shift values relative to samples obtained from the fresh catalyst and no apparent "extracrystalline signals" were observed. It is noted that ^{129}Xe NMR is relatively insensitive in probing the *extracrystalline* (or *intercrystalline*) environments of zeolites (43) whose average pore dimension normally exceeds the size of the Xe atom by more than two to three orders of magnitude. If Xe atoms were located in such an environment, they would contribute to the ^{129}Xe NMR resonance typically in the 5–30 ppm range in the chemical shift (44). Thus, the above results indicate that the ^{129}Xe resonance arises from xenon adsorbed within the

intracrystalline channels of the ZSM-5 zeolite which also contain coke residues. In addition, samples S1, S3, and S4 yielded spectra (Figs. 4b, 4d, and 4e, respectively) with multiple features and broader overall linewidth as compared to those obtained from S2 and S5 (Figs. 4c and 4f, respectively), indicating an inhomogeneous distribution of coke in the former samples. The slight decrease in the overall ^{129}Xe chemical shift in S3 compared to the other samples is due to the relatively low xenon coverage (θ) and hence a relative high coke content in the sample (Table 1), as is also indicated by a low xenon adsorption in Fig. 3. A similar behavior is also found for the spectrum of sample T3 (Fig. 4i). Accordingly, for samples S3 and T3, an extended number of signal accumulations is necessary in order to obtain a spectrum with adequate signal-to-noise (S/N) ratio.

The results also show that the internal coke distribution is more homogeneous for samples in the presence of H_2 than N_2. For the latter case, light volatile soft coke may form within the intracrystalline voids of the zeolite (25) resulting in an inhomogeneous broadening of the ^{129}Xe resonance. This internal coke may effectively be removed when exposed to H_2, resulting in a slightly broader (compared to the fresh zeolite) but more homogeneous ^{129}Xe line with a chemical shift similar to that of the fresh catalyst.

The conclusions deduced from the spectral analyses of the coked samples can be summarized as follows. First, all spectra show the presence of some amount of internal coke residues which correlate nicely with the TGA and xenon adsorption data. Second, a more homogeneous coke distribution and a more efficient regeneration of the catalyst are found when the reaction is carried out in the presence of H_2 than in N_2.

Along with the information deduced from the detailed lineshape and linewidth analyses, complementary information may also be obtained from the variations of the ^{129}Xe NMR chemical shift with Xe loading, as shown in Fig. 5. Only the chemical shift value corresponding to the major peak in each spectrum is depicted in Fig. 5 in order to avoid complicity in the figure. The upward concave dependence of the chemical shift at low Xe loading is attributed to the presence of strong adsorption sites (43, 45) and/or a broad distribution of the adsorption sites (46). Although such behavior has been found in many M^{+2} ion-exchanged zeolites (43, 45–48) and in ZSM-5 zeolites (13, 49, 50), our understanding of this phenomenon is far from being complete. Nevertheless, our results obtained from ^{27}Al MAS NMR experiments indicate that no additional extra-framework Al is present in the aged catalyst. Further treatment of the samples with acetylacetone (acac) for five days (40–42) also revealed no trace of "invisible Al." It is noted that in this context we are more interested in the variations in the slope of the chemical shift curve at high Xe uptake (*vide infra*) rather than the value of the intercept. Accordingly, the observed ^{129}Xe NMR chemical shift in Fig. 5 can be described

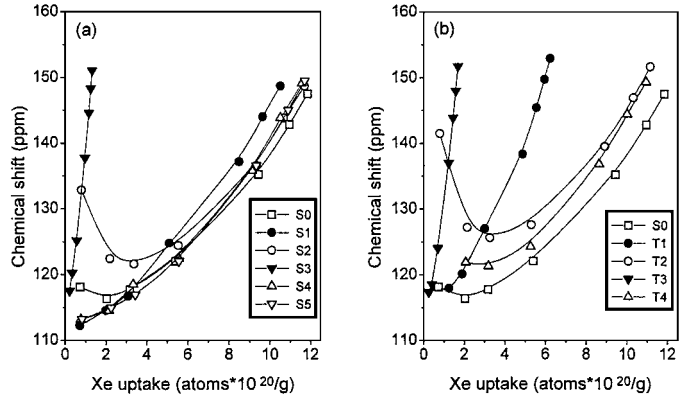

FIG. 5. Variation of the ^{129}Xe NMR chemical shift (obtained at room temperature) with xenon loading for fresh and coked samples obtained from (a) the five-stage process and (b) the control experiments. The sample notations (Table 1) and symbols are identical to that shown in Fig. 3. Note that, for the purpose of simplification and easy comparison of the data, only the chemical shift values of the main resonance peak were plotted despite the fact that some of the samples showed multiple resonance lines at low Xe loading (see Fig. 4).

by the linear equation (43)

$$\delta(\rho) = \delta_o + \delta_s(\rho = 0) + \sigma_{xe} \cdot \rho, \qquad [2]$$

where $\delta_o = 0$ is the reference and ρ represents the Xe density. The term $\delta_s(\rho = 0)$ is the chemical shift at zero Xe loading whose value can readily be obtained by extrapolating the straight line (at higher Xe loading) to the chemical shift axis. The thus obtained value of $\delta_s(\rho = 0)$ is the sum of two contributions, namely the part arising from interactions between Xe and the zeolite walls and the part from interactions between Xe and coke residues. The last term in Eq. [2], which predominates at higher Xe loading, characterizes the binary collisions between two xenon atoms and is proportional to the density of the adsorbed Xe. The slope of the plot $\delta(\rho)$ vs ρ therefore yields σ_{xe} which is inversely proportional to the effective internal pore volume of the zeolite (13, 23, 43, 46, 49, 51). An increase in σ_{xe}, therefore, reflects an increase in the internal coke content at the expense of the internal free volume.

The relative change of the free volume can be expressed as (13, 23, 49)

$$V/V_o = (\sigma_{xe})_{fresh}/(\sigma_{xe})_{coked}, \qquad [3]$$

where V is the internal volume of the coked sample and V_o is the internal volume of the fresh sample. Taking the experimental value of $(\sigma_{xe})_{fresh} = 5.10 \times 10^{-20}$ ppm g cat. atom^{-1} obtained from the fresh sample, the residual free volume for all coked samples can be calculated according to Eq. [3]. The results are summarized in Table 1.

Accordingly, mild internal coking was found at the end of Stage I (sample S1) resulting in a decrease (ca. 11%) in internal free volume compared to the fresh zeolite. However, most of the internal coke is effectively removed during Stage II as indicated by the nearly full recovery of the internal free volume ($V/V_o = 99.2\%$). Thus it is concluded that nearly all of the coke (total content 5.3 wt%) present in sample S2 is located on the external surface of the zeolite crystallites. During Stage III, coke continues to build up simultaneously in the internal channels and the external surfaces of the zeolite in the presence of N_2 at 813 K. Thus, a nearly complete blocking of internal pores results, as indicated by the drastic decrease in effective free volume and adsorption capability for xenon. Upon switching the carrier gas from N_2 to H_2 in Stage IV, the internal coke is preferentially removed as compared to external coke, hence resulting in a substantial free volume recovery of sample S4. As the reaction continued to 753 K in Stage V under H_2, a slight decrease in free volume was observed under extended TOS.

The same analysis can also be made for samples obtained from the control experiments and the results are also shown in Table 1. A simple comparison of the coke content (or V/V_o) data between the test samples (T1–T4) and the samples obtained from the corresponding stage of the five-stage selectivation process (S1–S4) indicate that prolonged TOS favors the formation of internal coke. Furthermore, a detailed data comparison between those from samples T2 and T4 further reflect that, in the presence of H_2, lowering of the reaction temperature tends to promote the formation of internal coke, whereas the external coke is more preferentially formed at higher temperatures.

The surface C/Si ratio of each sample was examined by X-ray photoelectron spectroscopy; the results are also summarized in Table 1. We found that the values of the C/Si ratio for samples obtained at different stages follow the order S3 > S5 > S4 > S1 > S2. The trend is similar to the variation of coke content obtained from TGA and obtained from Xe adsorption which indicated that, under H_2 treatment, the internal coke was removed preferentially as compared to the external coke. This observation is in line with the result recently reported by Jong *et al.* (50). In their study of the regeneration of coked H–ZSM-5 catalysts obtained during ethylbenzene disproportionation, the authors disclosed that, during the initial stage of regeneration, internal coke was effectively removed (through hydrocracking reactions) in the presence of H_2. On the other hand, for the external coke, only partial hydrocracking of bulky alkyl polyaromatics took place upon regeneration under H_2. As a result, the authors also observed an increase in *p*-diethylbenzene selectivity.

Ammonia TPD experiments were performed to investigate the variation of zeolite acidity during the reaction. The results are presented in Fig. 6. All TPD profiles exhibit two desorption peaks located at about 473 and 643 K with the exception of samples S3 and T3. In these two cases, only a single peak was observed at low temperature. The two desorption peaks appearing at 473 and 673 K can be assigned to the desorption of NH_3 from weak and strong acid sites, respectively. The apparent shift of the desorption peak toward a higher temperature upon reaction (not found for samples S3 and T3) indicates that the strong acid sites play a more active role during the reaction. Presumably, the relative concentration of the strong and weak acid sites in each sample can be obtained by the ratio of the two integrated peak areas. However, a more qualitative description of the change in acidity during the reaction is presented here. It is worthwhile to mention that, in comparison with the fresh catalyst, all spent samples exhibit a notable reduction in desorption peak areas (hence the number of acid sites) upon reacting with toluene (Fig. 6). Apparently, the strong acid sites suffer a more drastic decrease in peak area (more than 40%) than the weak acid sites (only ca. 10%). For samples obtained under N_2 atmosphere (i.e., samples S1, S3, T1, and T3), the overall residual amount of acidity is less than that obtained under H_2 carrier gas (i.e., samples S2, S3, S5, T2, and T4). Samples S3 and T3, which were most severely aged, exhibit not only a drastic decrease in the overall acidity but also an elimination of the strong acid sites. Upon switching the carrier gas from N_2 to H_2, the increase in the overall acidity mainly arises from the removal of the internal coke and hence the recovery of the internal acid sites.

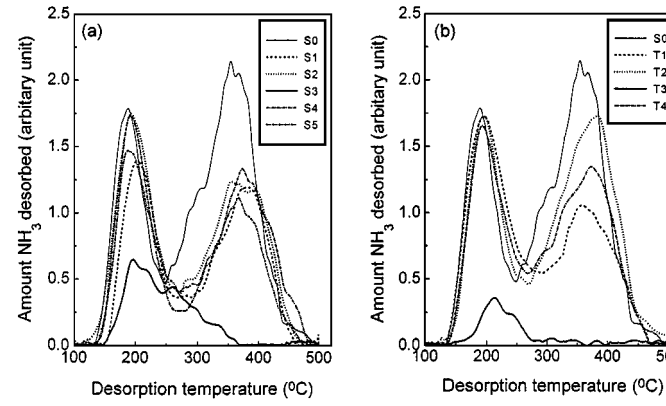

FIG. 6. Ammonia TPD profiles of the fresh and coked samples obtained from (a) the five-stage process and (b) the control experiments. The detailed reaction conditions and the corresponding sample notations are given in Table 1.

It has been suggested by many researchers (31–39) that the high *para*-selectivity obtained from the modified ZSM-5 during toluene disproportionation is mainly caused by product selectivity. This argument is true only when the pore openings of the ZSM-5 zeolites can be suitably reduced to ensure a predominate yield in *para*-isomers. However, it was found (31) that the rate of *para*-xylene isomerization on the external sites of the zeolite crystals is typically three to four orders of magnitude faster than that for the

disproportionation reaction. Since an equilibrium mixture of product isomers should be obtained even at low conversions (31, 52, 53), the external surface acid sites therefore must be substantially poisoned (or deactivated) to prevent re-isomerization (which in turn reduces *para*-selectivity) on the external surfaces of the zeolite crystallites. The deactivation of surface acidity is commonly accomplished by surface modification such as chemical vapor deposition (CVD) of silicon (17, 54, 55). Since the size of the typical silicon source molecules, e.g., tetraalkyl orthosilicate ($Si(OR)_4$, where R represents an alkyl group that contains one to four carbon atoms), are larger than the channel aperture of the ZSM-5 zeolite, they can only react with the external acid sites or sites close to the pore mouth. The drawback of the Si-deposition method is that while it is practical in deactivating the external acid sites, the deposited silicon also tends to narrow the pore mouth to a certain extent (56). Alternatively, such catalyst–surface modification can also be achieved by the coking process (17). The five-stage coke selectivation process described in this report is employed for the same purpose.

Carbonaceous deposit is known to build up simultaneously in the intracrystalline channels and on the extracrystalline surfaces of the ZSM-5 zeolite during catalytic reactions. For example, in the study of coking during ethylbenzene disproportionation over a H–ZSM-5 zeolite, Chen *et al.* (13) revealed (based on their NH_3-TPD and IR results) that, during the initial stage of reaction, coke tends to deposit preferentially on the Brønsted acid sites located within the zeolite channels rather than on the weaker external sites. Accordingly, a notable decrease in the catalytic activity and effective free volume of the catalyst was found. The authors also demonstrated that, as the total coke content exceeds ca. 7 wt%, the residual activity and effective free volume of the catalyst remains nearly constant ($V/V_o = 83\%$) and the deposition of external coke becomes predominant. Similarly, in the present study, the ^{129}Xe NMR results deduced from sample S1 (total coke content 7.2 wt%) also reveal a ca. 11% decrease in the effective free volume ($V/V_o = 88.5\%$; Table 1), and the coke is distributed rather inhomogeneously (Fig. 4b) inside the channels. It should be noted that, in the work of Chen *et al.* (13), the study was done on a bulkier reactant and at a much lower temperature (573 K). Thus, the slightly larger effective free volume found in the present system may be due to the fact that external coke is preferentially formed at elevated temeperatures; this is consistent with the finding disclosed earlier (*vide supra*). The formation of coke during Stage I resulted in a monotonous decrease in toluene conversion from the initial value of about 45 to about 38 wt%, while the *para*-xylene selectivity remained practically unchanged at ca. 24%.

An interesting question which concerns the relative concentration of the internal and the external acid sites deserves to be addressed at this point. It is worthwhile pointing out that, in this context, the term "acidity" cannot be readily defined on a molecular level. For example, the number of acid sites, which are indicated by a probe, should also depend on the size and physical/chemical properties of the probe molecules used for the measurement. The problem becomes even more serious when the measurement of the external acidity alone is concerned (57). Nonetheless, it is generally accepted that the number of external surface sites should increase with decreasing crystalline size of the catalyst (57–59). For example, Melson and Schüth (59) have recently disclosed that the percentage of "external acid sites" increased from 3.9 to 60.5% of the total number of acid sites as the size of the zeolite crystallites decreased from 5–10 to 0.1 μm by using 2,6-dimethylpyridine as the probe molecule. Incidentally, the properties of the H–ZSM-5 zeolite (Si/Al = 34, crystalline size ca. 0.3–0.6 μm) used in the present study are rather similar to the small crystals (Si/Al = 35, crystalline size ca. 0.1 μm) used in Ref. (59). Thus, it is probably not surprising that a comparable amount of internal and external acid sites exist in our fresh sample.

During Stage II, the H_2 gas acts as an effective regenerating medium, which reacts with the coke residues or the coke precursors through hydrogenation or hydrocracking. It has been shown (13, 50) that the strong Brønsted acid sites, which are believed to be located mostly in the internal ZSM-5 channels, play the key role during both initial deactivation and initial regeneration. Shielding and/or poisoning of the strong acid sites by coking are found to be responsible for the initial catalyst deactivation. During initial regeneration, it is also the internal strong acidity that is preferentially recovered compared to the surface sites. As a result, the internal coke is effectively removed during Stage II, and hence the observed amount of residual coke (5.3%) can be ascribed mostly due to the external coke. This is supported by the nearly complete recovery (compared to the fresh catalyst) of the internal free volume ($V/V_o = 99.2\%$). However, since the amount of external coke was not sufficient to thoroughly cover the remaining external acid sites of the zeolite crystallites, no significant *para*-selectivity enhancement was found during Stage II.

In Stage III, more severe reaction conditions were adopted to accelerate coking. This resulted in a marked increase in the coke content and a marked S-shape decrease in toluene conversion. At the beginning of Stage III, while the carrier gas was switched from H_2 to N_2, the sharp increase in toluene conversion (from ca. 44 to 52 wt%) is due to the sudden increase in the reaction temperature. Separate control experiments showed that the rate of initial deactivation increased more than three fold as the reaction temperature was increased from 753 to 813 K (*vide supra*). Moreover, no significant change in *para*-selectivity was observed except until the toluene conversion level dropped below ca. 25 wt% under the N_2 atmosphere (Figs. 2a and 2c).

Similarly, during Stage III of the five-stage selectivation process, a notable increase in *para*-selectivity was found to occur at conversions lower than ca. 25 wt%. It is proposed that during Stage III a continuous coke deposition occurs simultaneously in the intracrystalline channels and on the extracrystalline surfaces of the ZSM-5 zeolite. The nature of the internal coke is probably that of light volatile hydrocarbons, which can easily undergo hydrocracking in the presence of H_2 (for example, during the succeeding Stage IV). As this coke continues to accumulate inside the zeolite channels, the possibility of pore blocking also is increased with increasing TOS and in turn causes more coke to form on the external surface of the zeolite crystallites. As the conversion nears the threshold of its S-shape reflection point at ca. 25 wt% (see Fig. 1), a nearly complete coverage of the external acid sites by coking is reached, and the pore openings are also somewhat narrowed hence resulting in a sharp increase in the *para*-selectivity. In the meantime, the conversion gradually decreases. The complete blocking of the external acid sites by coking is therefore a crucial threshold for *para*-selectivity enhancement. At the end of Stage III, when the toluene conversion reaches its lowest value (5.4 wt%), the *para*-xylene selectivity also reaches its highest value of 47%.

In Stage IV, the introduction of the H_2 carrier gas effectively reactivated the catalyst by removing most of the internal (and some of the external) coke through hydrogenation or hydrocracking reactions. The sharp increase in conversion during Stage IV is mainly due to the recovery of the internal acidity, whereas the rapid decrease in *para*-selectivity may be ascribed to the partial removal of the external coke and hence the partial recovery of surface acid sites. Since ca. 93.8% of the internal free volume was recovered at the end of Stage IV, it is assumed that only a small portion of the total coke (out of the total amount of 18.3 wt%) was contributed by the internal coke. Apparently, the external coke is more difficult to remove even by H_2 as the regenerating gas. Thus, unlike the light volatile soft coke which tends to deposit within the intracrystalline voids, the coke deposited on the external surfaces is probably more bulkier, less volatile hard coke of polyaromatic nature (49). Consequently, the activity of the catalyst is not fully recovered as evidenced by the lower conversion at the end of Stage IV compared to that at the beginning of Stage III.

In the final stage, the reaction was carried out at a lower temperature (753 K), while maintaining under the H_2 environment. This resulted in a sudden decrease in conversion and a sharp increase in *para*-selectivity at the beginning of Stage V. Moreover, as the reaction continued, the rate of coking and/or the rate of coke removal (under H_2 as regenerating gas) appeared to be slowing down. The reaction appeared to have reached a steady state by which the conversion was maintained at ca. 33 wt%, while the *para*-selectivity leveled off at ca. 49%. The five-stage process described in this report, therefore, provides an effective way of modifying the external surfaces of the H–ZSM-5 zeolite by external coking in a manner similar to the effect of surface modification by Si-CVD. As a result, the secondary isomerization pathways of *para*-xylene may be greatly reduced which in turn enhances the *para*-selectivity while maintaining a reasonable conversion.

CONCLUSIONS

We have demonstrated a unique five-stage process, which can enhance the selectivity of *para*-xylene by selective coking during toluene disproportionation over H–ZSM-5 zeolite. As a result, we were able to achieve a two fold increase (from ca. 24 to 49%) in the *para*-xylene selectivity at a tolerable expense of toluene conversion (decrease from ca. 45 to 33 wt%). Based on the results obtained from the present study, the mechanism of coke selectivation is also described. In the presence of N_2 as a carrier gas, light volatile soft coke and/or coke precursors prefer to deposit inhomogeneously within the intracrystalline channels of the zeolite and are responsible for the decrease in toluene conversion. This internal coke may be effectively removed when H_2 is used as a carrier gas. Coke that tends to deposit on the external surface of the zeolite is mostly bulky hard coke. This coke is more difficult to remove by simple H_2 treatment. As a result, this external coke effectively modifies the surface acid properties of the zeolite crystallites which in turn cut off the secondary isomerization pathways of *para*-xylene, thus enhancing the *para*-selectivity.

ACKNOWLEDGMENTS

The authors thank the reviewers for their helpful comments and thank Prof. S. Cheng and Drs. T. H. Chang, S. J. Jong, and J. F. Wu for technical and instrumental supports. The financial supports of this work from the National Science Council of Republic of China (IW: NSC87-2214-E-007-005; SBL: NSC87-2113-M-001-003) are gratefully acknowledged.

REFERENCES

1. Rollman, L. D., *J. Catal.* **47**, 113 (1977).
2. Rollman, L. D., and Walsh, D. E., *J. Catal.* **56**, 139 (1979).
3. Bibby, D. M., Milestone, N. B., Patternson, J. E., and Aldridge, L. P., *J. Catal.* **97**, 493 (1986).
4. Magnoux, P., Cartraud, P., Mignard, S., and Guisnet, M., *J. Catal.* **106**, 242 (1987).
5. Moljord, K., Magnoux, P., and Guisnet, M., *Appl. Catal., A* **122**, 21 (1995).
6. Lopes, J. M., Lemos, F., Ribeiro, F. R., Derouane, E. G., Magnoux, P., and Guisnet, M., *Appl. Catal., A* **114**, 161 (1994).
7. Behrsing, T., Jaeger, H., and Sanders, J. V., *Appl. Catal., A* **54**, 289 (1989).
8. Uguina, M. A., Serrano, D. P., Grieken, R. V., and Vènes, S., *Appl. Catal., A* **99**, 97 (1993).
9. Corma, A., Miguel, P. J., and Orchillés, A. V., *Appl. Catal., A* **117**, 29 (1994).

10. Choudhary, V. R., Sivadinarayana, C., Kinage, A. K., Devadas, P., and Guisnet, M., *Appl. Catal., A* **136**, 125 (1996).
11. Snape, C. E., McGhee, B. J., Andresen, J. M., Hughes, R., Koon, C. L., and Hutchings, G., *Appl. Catal., A* **129**, 125 (1995).
12. Liang, W., Jin, Y., Yu, Z., Wang, Z., Han, B., He, M., and Min, E., *Zeolites* **17**, 297 (1996).
13. Chen, W. H., Jong, S. J., Pradhan, A., Lee, T. Y., Wang, I., Tsai, T. C., and Liu, S. B., *J. Chin. Chem. Soc.* **43**, 305 (1996).
14. De Lucas, A., Canizares, P., Durán, A., and Carrero, A., *Appl. Catal., A* **156**, 299 (1997).
15. Holmes, S. M., Garforth, A., Maunders, B., and Dwyer, J., *Appl. Catal., A* **151**, 355 (1997).
16. Choudhary, V. R., Kinage, A. K., Sivadinarayana, C., Devadas, P., Sansare, S. D., and Guisnet, M., *J. Catal.* **158**, 34 (1996).
17. Čejka, J., Zilková, N., Wichterlová, B., Eder-Mirth, G., and Lercher, J. A., *Zeolites* **17**, 265 (1996).
18. Guisnet, M., and Magnoux, P., *Catal. Today* **36**, 477 (1997).
19. Bhatia, S., Beltramini, J., and Do, D. D., *Catal. Rev.-Sci. Eng.* **31**, 431 (1989-90).
20. Bibby, D. M., Howe, R. F., and McLellan, G. D., *Appl. Catal., A* **93**, 1 (1992).
21. Karge, H. G., *Stud. Surf. Sci. Catal.* **58**, 531 (1991).
22. Guisnet, M., and Magnoux, P., *Appl. Catal.* **54**, 1 (1989).
23. Pradhan, A., Lin, T. S., Chen, W. H., Jong, S. J., Wu, J. F., Chao, K. J., and Liu, S. B., *J. Catal.*, in press (1999).
24. Sotelo, J. L., Uguina, M. A., Valverde, J. L., and Serrano, D. P., *Appl. Catal.* **114**, 273 (1994).
25. Chen, W. H., Pradhan, A., Jong, S. J., Lee, T. Y., Wang, I., Tsai, T. C., and Liu, S. B., *J. Catal.* **163**, 436 (1996).
26. Absil, R. P. L., Butt, J. B., and Dranoff, J. S., *J. Catal.* **92**, 187 (1985).
27. Guisnet, M., *J. Catal.* **88**, 249 (1984).
28. Karge, H. G., Wada, Y., Weitkamp, J., and Jacobs, P. A., *J. Catal.* **88**, 251 (1984).
29. Schulz-Ekloff, G., Jaeger, N. I., Vladov, C., and Petrov, L., *Appl. Catal.* **33**, 73 (1987).
30. Bauer, F., Ernst, H., Geidel, E., and Schodel, R., *J. Catal.* **164**, 146 (1996).
31. Chen, N. Y., Degnan, T. F., Jr., and Smith, C. M., "Molecular Transport and Reaction in Zeolites: Design and Application of Shape Selective Catalysts," VCH, Weinheim/New York, 1994.
32. Haag, W. O., Olson, D. H., and Rodewald, P. G., U.S. Patent 4,358,395, 1982.
33. Haag, W. O., Olson, D. H., and Rodewald, P. G., U.S. Patent 4,508,836, 1985.
34. Beck, J. S., McCullen, S. B., and Olson, D. H., U.S. Patent 5,365,004, 1994.
35. Beck, J. S., Olson, D. H., and McCullen, S. B., U.S. Patent 5,367,099, 1994.
36. Young, L. B., Butter, S. A., and Kaeding, W. W., *J. Catal.* **76**, 418 (1982).
37. Kürschner, U., Jerschkewitz, H. G., Schreier, E., and Völter, J., *Appl. Catal.* **57**, 167 (1990).
38. Babu, G. P., Santra, M., Shiralkar, V. P., and Ratnasamy, J., *J. Catal.* **100**, 458 (1986).
39. Beschmann, K., and Riekert, L., *J. Catal.* **141**, 548 (1993).
40. Bosaček, V., Freude, D., Fröhlich, T., Pfeifer, H., and Schmiedel, H., *J. Colloid Interface Sci.* **85**, 502 (1982).
41. Engelhardt, G., and Michel, D., "High-Resolution Solid-State NMR of Silicates and Zeolites," Chap. V. Wiley, New York, 1987.
42. Deng, F., Yue, Y., and Ye, C., *J. Phys. Chem. B* **102**, 5252 (1998), and references therein.
43. Fraissard, J., and Ito, T., *Zeolites* **8**, 350 (1988).
44. Liu, S. B., Wu, J. F., Ma, L. J., Lin, M. W., and Chen, T. L., *Coll. Czech. Chem. Commun.* **57**, 718 (1992).
45. Cheung, T. T. P., Fu, C. M., and Wharry, S., *J. Phys. Chem.* **92**, 5170 (1988).
46. Cheung, T. T. P., *J. Phys. Chem.* **93**, 7549 (1989).
47. Ito, T., and Fraissard, J., *J. Chem. Phys.* **76**, 5225 (1982).
48. Liu, S. B., Fung, B., Yang, T. C., Hong, E. C., Chang, C. T., Shih, P. C., Tong, F. H., and Chen, T. L., *J. Phys. Chem.* **98**, 4393 (1994).
49. Pradhan, A. R., Wu, J. F., Jong, S. J., Chen, W. H., Tsai, T. C., and Liu, S. B., *Appl. Catal., A* **159**, 187 (1997).
50. Jong, S. J., Pradhan, A. R., Wu, J. F., Tsai, T. C., and Liu, S. B., *J. Catal.* **174**, 210 (1998).
51. Johnson, D. W., and Griffiths, L., *Zeolites* **7**, 484 (1987).
52. Kaeding, W. W., Chu, C., Young, I. B., and Butter, S. A., *J. Catal.* **69**, 392 (1981).
53. Meshram, N. R., Hedge, S. G., and Kulkarni, S. B., *Zeolites* **6**, 434 (1986).
54. Wang, I., Ay, C. L., Lee, B. J., and Chen, M. H., *Appl. Catal.* **54**, 257 (1989).
55. Kim, J. H., Ishida, A., Okajima, M., and Niwa, M., *J. Catal.* **161**, 387 (1996).
56. Kim, J. H., Namba, S., and Yashima, T., *Appl. Catal., A* **83**, 51 (1992).
57. Karge, H. G., Kösters, H., and Wada, Y., "Proceedings, 6th International Zeolite Conference" (D. H. Olson and A. Bisio, Eds.), p. 308. Butterworths, London, 1984.
58. Kaeding, W. W., *J. Catal.* **95**, 512 (1985).
59. Melson, S., and Schüth, F., *J. Catal.* **170**, 46 (1997).